Bull. Mater. Sci., Vol. 37, No. 3, May 2014, pp. 685–693. © Indian Academy of Sciences.

Development of a new solid-state absorber material for dye-sensitized solar cell (DSSC)

SWAPNA LILLY CYRIAC[1], B DEEPIKA[1], BHASKARAN PILLAI[2], S V NAIR[1,*] and K R V SUBRAMANIAN[1,*]

[1]Amrita Centre for Nanosciences and Molecular Medicine, Ponekkara P.O., Kochi 682 041, India
[2]Department of Radiation Oncology, AIMS, Kochi 682 041, India

MS received 20 February 2013; revised 1 April 2013

Abstract. **In contrast to the conventional DSSC systems, where the dye molecules are used as light harvesting material, here a solid-state absorber was used as a sensitizer in conjunction with the dye. The materials like ZnO and $Al_2O_3:C$, which will show optically stimulated luminescence (OSL) upon irradiation were used as extremely thin absorber layers. This novel architecture allows broader spectral absorption, an increase in photocurrent, and hence, an improved efficiency because of the mobility of the trapped electrons in the absorber material after irradiation, to the TiO_2 conduction band. Nanocrystalline mesoporous TiO_2 photoanodes were fabricated using these solid-state absorber materials and after irradiation, a few number of samples were co-sensitized with N719 dye. On comparing both the dye loaded photoanodes (ZnO/TiO_2 and $Al_2O_3:C/TiO_2$), it can be concluded from the present studies that, the $Al_2O_3:C$ is superior to ZnO under photon irradiation. $Al_2O_3:C$ is more sensitive to photon irradiation than ZnO and hence there can be more trap centres produced in $Al_2O_3:C$.**

Keywords. **Optically stimulated luminescence; DSSC; zinc oxide; carbon-doped aluminium oxide.**

1. Introduction

The need for alternative energy sources led to tremendous research work particularly those using nanomaterial, in the area of third generation photovoltaic systems to pull the efficiency from reported 11·1% (O'Regan and Grätzel 1991) to the predicted theoretical value of 63% (Luque and Martin 1997). The most important problems that are faced in the DSSC, leading to low efficiency, are the recombination of the photo-injected electrons (Ghada *et al* 2008) and the limited spectral absorption range or light harvesting (Gopal *et al* 2006). Thus, a key to improve the efficiency is to increase the light harvesting property in DSSC, which can be achieved in different ways.

Currently organic dyes (Li *et al* 2006), semiconductor quantum dots (Nozik *et al* 2002; Schaller *et al* 2004), porphyrins (Graetzel *et al* 2003) or a combination of these forms the light-harvesting component (absorber material) of conventional DSSC's. However, these components still suffer from limitations of average light harvesting efficiencies and lack of lifetime/stability. A promising alternative is to develop a new solid-state absorber material, which upon high-energy irradiation shows OSL (optically stimulated luminescence) property by adequately populating trap levels that can hold electrons for indefinite time. These electrons, which normally luminesce by recombination, are readily available for transport to the semiconductor region (in contact with the OSL layer) upon optical stimulation, thereby increasing the efficiency of the solar cell.

Optically stimulated luminescence (OSL) is the luminescence emitted from a pre-irradiated insulator or a semiconductor during exposure to light. During high-energy irradiation, the absorbed energy is partially transferred to the charges (electrons and holes) thereby creating free charge carriers within the material. Majority of these free carriers are trapped at pre-existing or radiation induced defect sites in the crystal lattice of the material, where they can remain for indeterminate periods of time. During optical stimulation with light, the trapped charges can be moved from the trap state into the conduction band and they recombine, and release energy consisting of luminescent light. Thus, irradiation creates a substantial electron population in the traps of the material (Schembri *et al* 2007). Materials showing OSL property can absorb wide spectral region because of the new trap centres formed. Combining the OSL material with the dye in DSSC can absorb vast spectral region thereby increasing the light harvesting property in DSSC.

The OSL material will emit luminescence after stimulation. If we quench this luminescence by transporting the

*Author for correspondence (krvsubramanian@aims.amrita.edu; shantinair@aims.amrita.edu)

trapped electrons from OSL material to semiconductor in the DSSC, we can increase the photocurrent even at lower energy stimulation. This OSL material on the working electrode can also act as a barrier layer to avoid the back flow of the electrons, reducing the recombination of the trapped electrons with the holes in the valence band (or holes in the electrolyte), thereby further increasing the efficiency. Materials showing crystal imperfections including point defects or interstitial defects, which can be created during synthesis or by doping, can show OSL property. Hence, OSL is a property of the solid-state material having high thermal and chemical stabilities, low effective atomic number, high sensitivity to radiation, high optical stimulation efficiency and wide bandgap allowing a large variety of stable traps and colour centres (Pradhan *et al* 2008).

To discuss the solid-state absorber materials chosen for this study, $Al_2O_3:C$ (carbon-doped Al_2O_3) and ZnO was chosen among various potential luminescent materials in view of its excellent OSL properties like low effective atomic number, favourable band width, etc. $Al_2O_3:C$ emits both RL and OSL in the blue region (420 nm). ZnO nanophosphors can be used as an OSL material because of the existence of intrinsic or extrinsic defects, high sensitivity and high optical stimulation efficiency as compared with other commercially available OSL materials (Cruz-Vaquez *et al* 2007). For these reasons, high-energy irradiated ZnO and $Al_2O_3:C$ used in conjunction with organic dyes can be strongly considered as promising candidates for the absorber material in the dye-sensitized solar cells (DSSC). The DSSC uses TiO_2 as the standard semiconducting layer for transport.

In our studies, to improve the efficiency of the current DSSC, the nanocrystalline ZnO and Al_2O_3 doped with carbon were synthesized using sol–gel method. The polycrystalline nanoparticles were coated on the conducting glass substrate and irradiated with ionizing radiation using a linear accelerator. This paper presents the OSL response and photovoltaic studies of the polycrystalline ZnO material and Al_2O_3 doped with carbon.

2. Experimental

2.1 *Synthesis of ZnO nanoparticles*

ZnO colloidal solution was prepared by a simple sol–gel method using zinc acetate dihydrate (extra pure, Merck) and sodium hydroxide (97%, Fisher Scientific) in methanol (Fisher Scientific) at 51 °C for 10 min. Sodium hydroxide solution was added drop-wise under high speed stirring for 30 min. The solution was sealed and centrifuged at 11000 rpm for 15 min. As obtained ZnO nanoparticles (NPs) were ultrasonically cleaned and re-suspended with methanol for 1 h. Cleaned colloidal solution of ZnO nanoparticles (NPs) were spin coated on TiO_2 thin film. The overall reaction can be written as:

$$Zn(CH_3COO)_2 + 2NaOH \rightarrow Zn(OH)_2 + 2CH_3COONa,$$

$$Zn(OH)_2 \text{ (unstable)} \rightarrow ZnO \text{ (stable)}.$$

By varying the concentration of NaOH, another set of stable ZnO nanocolloid was prepared.

2.2 *Preparation of TiO_2 thin film and ZnO/TiO_2 photoanode*

To form the TiO_2/ZnO/Ruthenium N719 photoanode structure, a TiO_2 (P25, Degussa) paste was prepared in ethanol and was coated on to cleaned fluorinated tin oxide glass (FTO glass, Solaronix) with 80% transmittance in the visible spectrum) by using a doctor blade technique. The film was calcined at 450 °C for 30 min to crystalline anatase form. The fresh ZnO nanocolloids were used for spin coating on TiO_2 mesoporous film at 1800 rpm in air for 5 min.

2.3 *Preparation of $Al_2O_3:C/TiO_2$ photoanode*

About 5 g of commercially available polycrystalline alumina powder (LR grade, NiCE), Al_2O_3 was first dissolved in ethoxy ethanol. Then, graphite fine powder (extra pure, Loba Chemie) was added slowly with a doping concentration of about 10000 ppm. Once the particles are dissolved in the solvent, the suspensions of $Al_2O_3:C$ was deposited on TiO_2 mesoporous thin film by doctor blade method. $Al_2O_3:C/TiO_2$ coated photoanode was dried in the furnace at a temperature of 450–500 °C in static air for 30 min.

2.4 *Irradiation of photoanode*

Optically-stimulated luminescence was studied at room temperature. All measurements were performed in a $20 \times 20 \times 2$ cm black acrylic phantom. The samples were irradiated with 6 MV photon beam and 15 MeV electron beam from an Elekta linear accelerator (Linac) for 25×25 cm field size. Since, Compton cross-section is more in 6 MV photon beam, it was chosen to create more trap centres in the samples. For 6 MV photon beam, OSL response was investigated for different absorbed doses (5 and 6 Gy) for each set of photoanode using an SSD technique with a 5 cm buildup block. 15 MeV electron beam was used only for ZnO/TiO_2 photoanode to deliver a 600 cGy with an appropriate built-up thickness.

2.5 *Cell fabrication*

A set of irradiated samples from both ZnO-coated TiO_2 and Al_2O_3-coated TiO_2 were immersed in 0·3 mM N719

dye (Solaronix Co. Ltd.) solution for 24 h of sensitization. The electrodes were dipped in such a way that only a portion of the substrate is sensitized with the dye. Along with the ETA sensitization, these half dye dipped samples will provide enough charge transport to the conduction band of TiO_2. So, our complete working electrode contains TiO_2-coated on FTO, irradiated ZnO or $Al_2O_3:C$ thin film sensitized with half dye. Pt-coated FTO was used as counter electrodes and the electrolyte was prepared as reported in the literature (Santiago *et al* 2009). Working and counter electrodes were sandwiched using a spacer of 60 μm thickness. Here, the active area of the cells was within 0·7–0·4 cm^2.

2.6 *Analytical techniques*

The prepared ZnO/TiO_2 thin film and $Al_2O_3:C/TiO_2$ thin-film substrates were characterized using a scanning electron microscope (SEM, JEOL, JSM-6490LA) and X-ray diffractometer (XPERT PRO, P Analytical). The photoluminescence (PL) measurements for both liquid and solid samples were performed with HORIBA, JOBIN YVON fluorometer (Model Fluoro Max 4). UV–Vis spectra were recorded on a PERKIN ELMER λ-750 spectrophotometer. The particle size was obtained using DLS (NICOMP TM 380 ZLS). The cyclic voltammetric (CV) measurements were performed using Autolab (PGSTAT302N). CV's were recorded at room temperature by employing a three-electrode cell with platinum as a counter electrode, sample as the working electrode and Ag/AgCl electrode as the reference electrode. The CV's were obtained by a continuous scanning from –2 V to +2 V at a scan rate of 0·05 to 0·01 V/s.

The current–voltage characteristics of the cells were measured using a digital source meter (Keithley Instruments Inc., Model 2420) under simulated AM 1·5 illumination provided by solar simulator (Newport, 92251A-1000, Oriel Instruments).

3. Results and discussion

The as-deposited film, figure 1(a), shows the amorphous nature of ZnO nanoparticles. Figure 1(b) shows the XRD of ZnO film annealed at 300 °C. The high crystallinity of this film shows that the thermal annealing has the effects on narrowing the diffraction peak, indicating that grain growth has occurred. Figure 1(c) shows XRD of ZnO coated over TiO_2. These films were annealed at 100 °C. Peaks corresponding to both TiO_2 and ZnO phases were observed in XRD spectra. The crystalline peaks of 27·77° and (34·9°, 36·7°) correspond to TiO_2 anatase and ZnO structures, respectively. All the peaks matched well with the bulk ZnO, which could be indexed as the zincite structure of ZnO (λ = 1·54056, quality: *C*, JCPDF no. 75-1526). The crystallinity of this TiO_2/ZnO composite was lower than that of ZnO and this may be due to the lower annealing temperature (100 °C). From XRD data, peaks at 34·9° and 36·7°, confirms the presence of ZnO nanoparticle formation, which was annealed at 300 °C. But, for the cell measurements, the amorphous ZnO coated on the TiO_2 was used. Though the high temperature treatment of ZnO thin film helps to improve the crystallinity of the film, it was observed that high temperature treatment initiated sintering of nanoparticles in the film with increase in particle size and also leading to a decrease in active surface area for the adsorption of dye molecule. Since, fine particle size (< 500 nm) is essential for demonstration of OSL property (Schembri *et al* 2007), the amorphous films were used for further studies and characterization.

In order to understand the uniformity of the coatings, SEM images of the thin films have been made. Figure 2 shows the surface morphology of the porous TiO_2 film and ZnO-coated TiO_2 film. Figure 2(b) demonstrates the formation of porous TiO_2 film, having high surface area. Figure 2(c) shows that thin layer of ZnO nanoparticles were formed on the surface of TiO_2. Using DLS (dynamic light scattering) analysis, the average hydrodynamic diameter for the two different concentrations (1 : 1 and 1 : 1·5) of the ZnO nanoparticles was found to be 17 and 34 nm, respectively (figure 3). The distribution was obtained by using number weighed NICOMP distribution. Figure 4(a) shows the room temperature photoluminescence spectra of ZnO methanol suspension. The samples were excited at 354 nm. The PL spectra show the emission peaks located at 397 and 544 nm correspond to UV and green emissions. The UV emission was due to the band-edge recombination of free excitons. The green

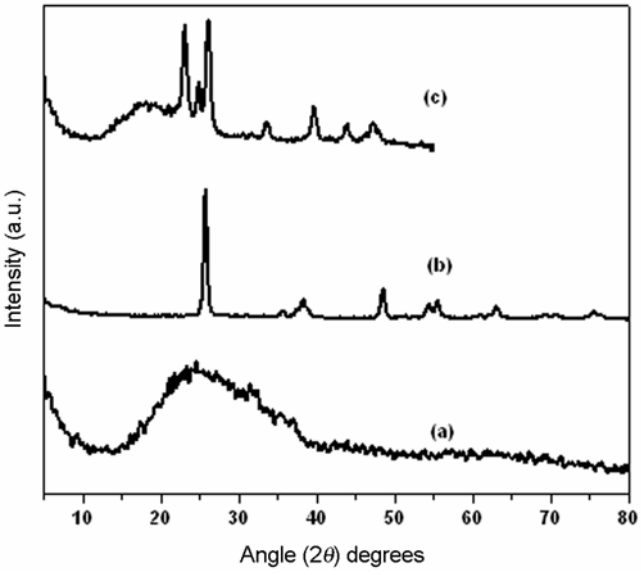

Figure 1. X-ray diffractograms of (**a**) amorphous ZnO, (**b**) crystalline ZnO and (**c**) ZnO coated over TiO_2.

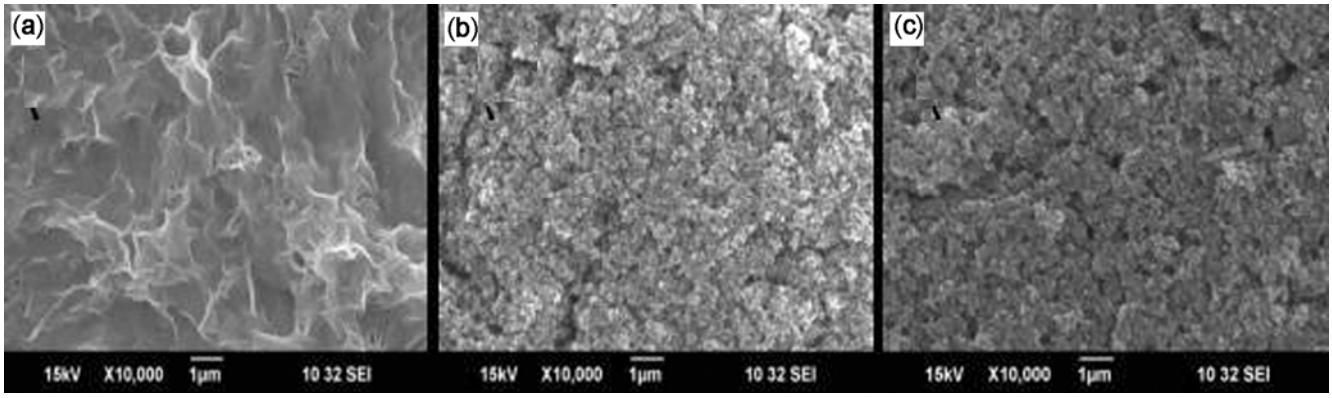

Figure 2. SEM images of (**a**) ZnO thin film, (**b**) mesoporous TiO_2 thin film and (**c**) ZnO coated TiO_2 thin film.

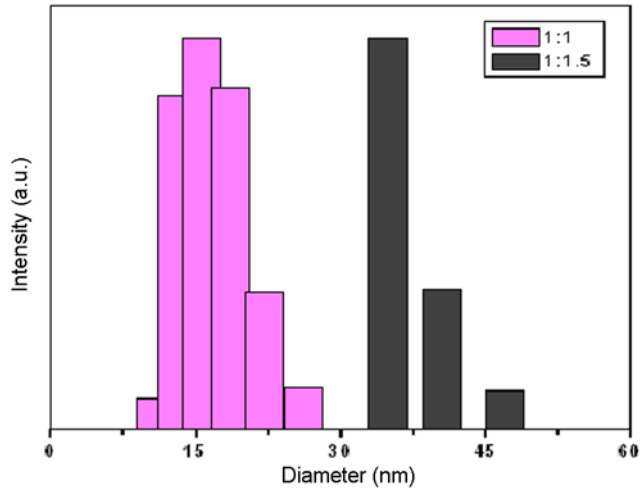

Figure 3. Particle size distribution of 1 : 1 and 1 : 1·5 ZnO nanocolloids.

emission at 544 nm was due to the oxygen vacancies and other defects.

The room temperature PL spectra of irradiated and non-irradiated amorphous ZnO thin film under excitation of 397 nm are shown in figure 4(b). The samples were irradiated with 15 MeV electron beam to deliver an absorbed dose of 600 cGy (centigray). In the emission spectra of the pristine samples ((a) and (b)), two main peaks were observed at 412 nm (violet emission) and 540 nm (green emission). But for the irradiated samples ((d) and (e)) with 15 MeV electron beam, it is observed that the position of the violet emission (412 nm) was affected by irradiation. A broad blue peak around 460 nm is observed for these samples. There was no shift in the green emission. But in the case of photon-irradiated sample (c), there was no shift in peak positions. On irradiating with 15 MeV electron beam, the knocked out electrons (due to inelastic collision) from the different atomic shells of the ZnO nanoparticles will be trapped either in these inherent defects centres or will create another defect centre in its electronic structure. As a result, there will be an either increase in the intensity of these inherent defect centre, due to the increased population of electrons in these levels, or will create another colour centre, due to the new defect level, in the PL spectra of ZnO nanoparticles. Here, the peak at 460 nm can be due to the new defect centre created by irradiation. The broadening of the peak may be due to the low electron density in that particular level. In addition to that, Compton effect, which is predominant in 6 MV photon beam is not energetically favourable to create radiation induced trap states in the ZnO lattice. Hence, there was no effect on the PL spectra.

The bandgap of ZnO nanocolloids was obtained by plotting the graph $(\alpha h\nu)^2$ vs $h\nu$ (figure 5). It was found that the ZnO nanocolloid in 1 : 1 ratio has a bandgap of 3·53 eV, whereas for 1 : 1·5 ratios, the E_g was reduced to 3·45 eV. From the XRD pattern (figure 6) of the alumina (Al_2O_3), graphite and Al_2O_3 : C thin films annealed at 500 °C, a shift in peak for the polycrystalline material doped with carbon was seen. The dopant, carbon, acts as a catalyst for the formation of defects in Al_2O_3 lattice. When the doping concentration increases, carbon atoms due to their smaller ionic radii (0·15 Å) occupies the interstitial positions and results in a lateral strain in Al_2O_3 lattice. Annealing the sample at 500 °C helps the fast diffusion of carbon atoms into Al_2O_3. In the figure, the 2θ position at 30·94 of Al_2O_3 has been shifted to 29·91, when it is doped with carbon. This negative shift ($\Delta\theta = 1{\cdot}03$) could be due to the lateral strain produced by the carbon atom in the Al_2O_3 lattice. The high intensity peak of graphite at 26·61 is not seen in the XRD pattern of Al_2O_3 : C. This could be due to low doping concentration (1 wt%) of carbon atom.

Figure 7 shows the SEM images of TiO_2 mesoporous film and Al_2O_3 : C/TiO_2 nano-composites. In figure 7(b), the morphology of Al_2O_3 : C is like a sheet on the surface of TiO_2 thin film due to the heat treatment at 450–500 °C. The room temperature PL emission spectra of Al_2O_3 : C thin film is shown in figure 8. All the samples were

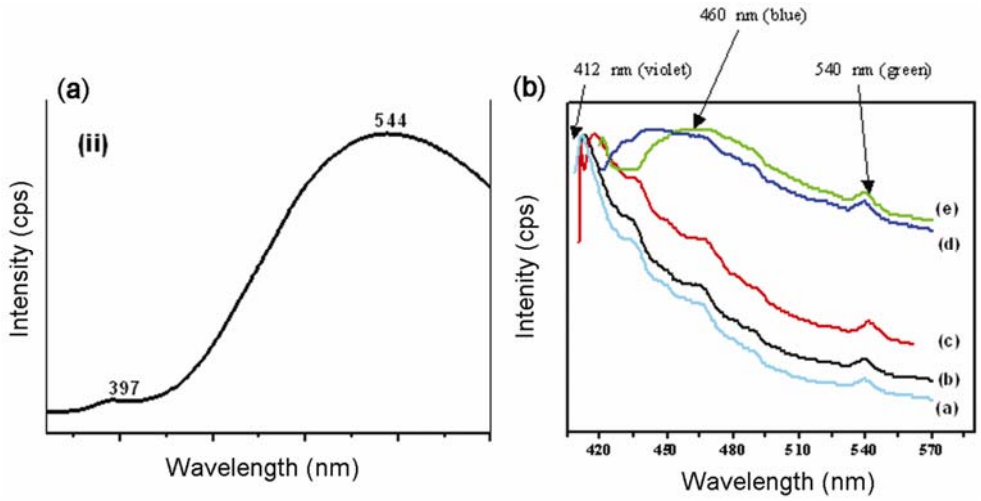

Figure 4. Photoluminescence spectra of (**a**) ZnO suspension and (**b**) ZnO thin film.

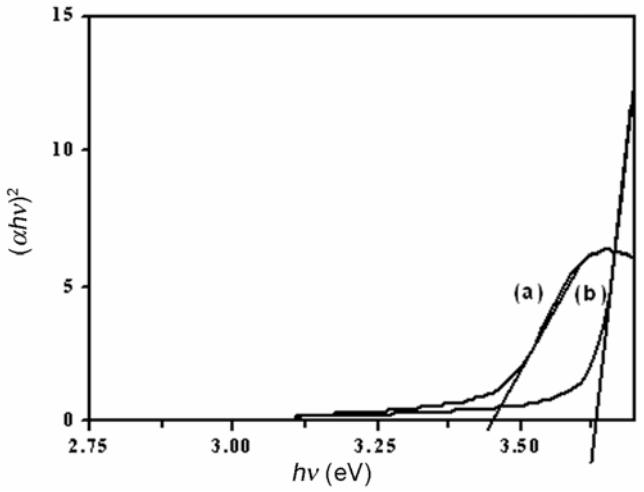

Figure 5. Bandgap determination of ZnO of colloidal suspension: (**a**) 1 : 1·5 and (**b**) 1 : 1.

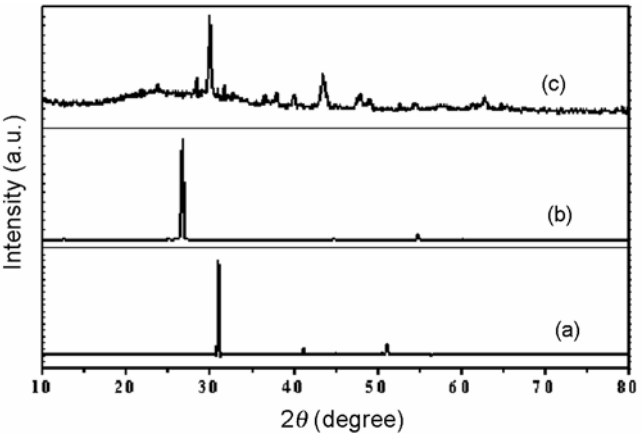

Figure 6. X-ray diffractograms of (**a**) Al_2O_3, (**b**) graphite and (**c**) Al_2O_3 : C.

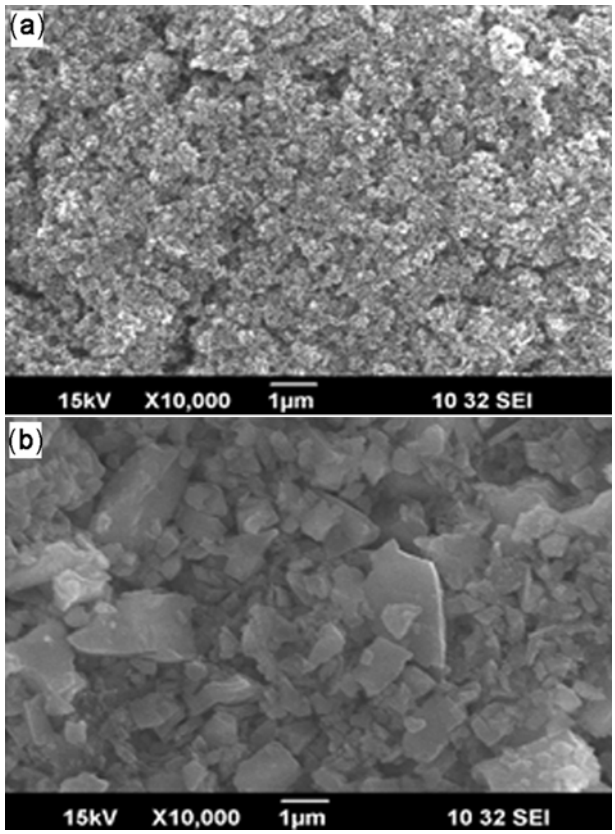

Figure 7. SEM images of (**a**) mesoporous TiO_2 thin film and (**b**) Al_2O_3 : C-coated TiO_2 film.

Table 1. HOMO and LUMO values of TiO_2, ZnO and Al_2O_3 by means of cyclic voltammetry.

	TiO_2	ZnO	Al_2O_3	N719 dye
LUMO (eV)	−3·870	−1·578	−2·716	−3·85
HOMO (eV)	−7·104	−5·108	−5·81	−5·45
E_g (eV)	3·234	3·53	3·094	

Table 2. Photovoltaic measurements of ZnO/TiO_2 composite with dye (N719).

Sample name	Cell details	V_{oc} (V)	J_{sc} (mA/cm^2)	Fill factor (%)	Efficiency (%)
Z1	Pristine	0·706	0·31	55	0·12
Z2	600 cGy (photon beam, 6 MV)	0·468	1	29	0·14
Z3	600 cGy (electron beam, 15 MeV)	0·5669	0·037	49·0407	0·010

Table 3. Photovoltaic measurements of ZnO/TiO_2 composite without dye.

Sample name	Cell details	V_{oc} (V)	J_{sc} (mA/cm^2)	Fill factor (%)	Efficiency (%)
Z4	Pristine (1 : 1)	0·634	0·603	50	0·19
Z5	600 cGy (Photon beam, 6 MV)	0·566	0·602	33	0·11
Z6	600 cGy (Electron beam, 15 MeV)	0·527	0·044	38	0·009

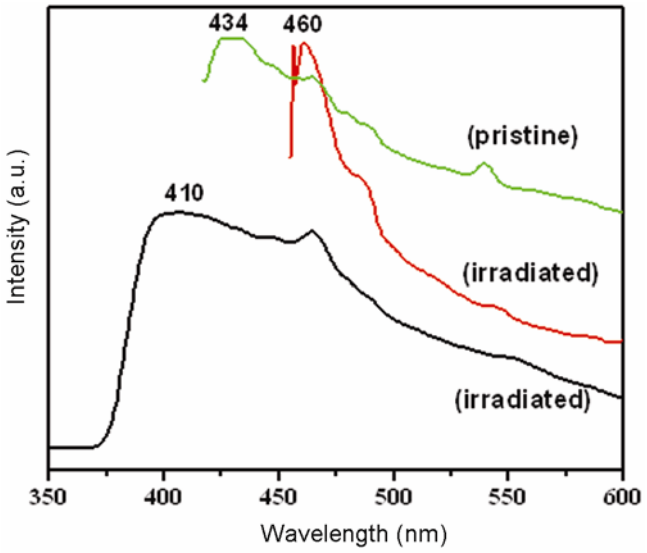

Figure 8. PL spectra of $Al_2O_3 : C$ (**a**) pristine sample and (**b**), (**c**) irradiated samples.

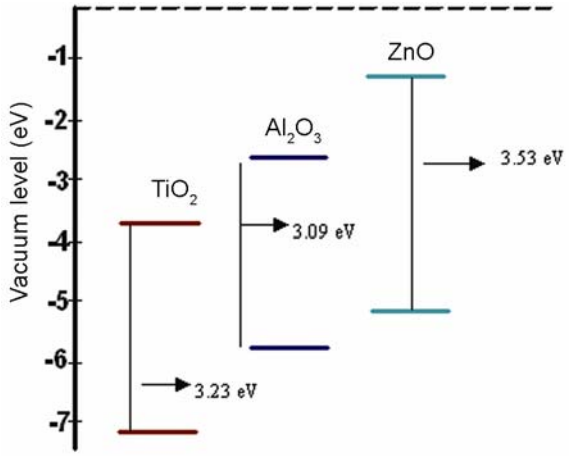

Figure 9. Schematic diagram of the electrochemically determined HOMO and LUMO of TiO_2, ZnO and Al_2O_3.

irradiated with 6 MeV photon beam to deliver an absorbed dose of about 600 cGy. The peaks at 410 and 461 nm in PL spectra correspond to F centre and F^- centre, respectively. The main OSL emission in $Al_2O_3 : C$ is due to F centre and F_2^+ centres (two oxygen vacancies with three electrons). F centre emission was obtained by excitation using 300 nm radiation (that corresponds to the F centre's excitation energy). $Al_2O_3 : C$ crystals contain a relatively high concentration of oxygen vacancies, V_0 that provides capture centres for electrons, like F-centres in alkali halide crystals. Here, the main emission centres are F-centres created by V_0 defect capturing two electrons, with the emission peak at $\lambda \sim 410$ nm. Hence, these results confirm that $Al_2O_3 : C$ thin film shows OSL property.

Table 1 outlines the band-off set values and bandgap of different semiconductors used for DSSC. The comparison of offset values between different semiconductors reveals that ZnO and Al_2O_3 are more electronegative than ZnO nanoparticles. Thus, it can be concluded that ZnO and Al_2O_3 can be used an extremely thin absorber (ETA) materials and can easily transfer electron from this ETA to the TiO_2 layer leading to an increase in the photocurrent and conversion efficiency. Figure 9 depicts schematically the electrochemically-determined energy levels of TiO_2, ZnO and Al_2O_3 on an electrochemical scale. This electron transfer is in addition to the role of the N719 dye, a well-established light harvesting organic molecule (Asha *et al* 2012). The dye, by itself, enhances the light harvesting and electron injection efficiencies of DSSC. DSSC contains thin layer of wide bandgap semiconductors, such as TiO_2 or ZnO. A schematic representation of DSSC is shown in figure 10. Its working principle is: (1) the incident photon is absorbed by the dye molecule

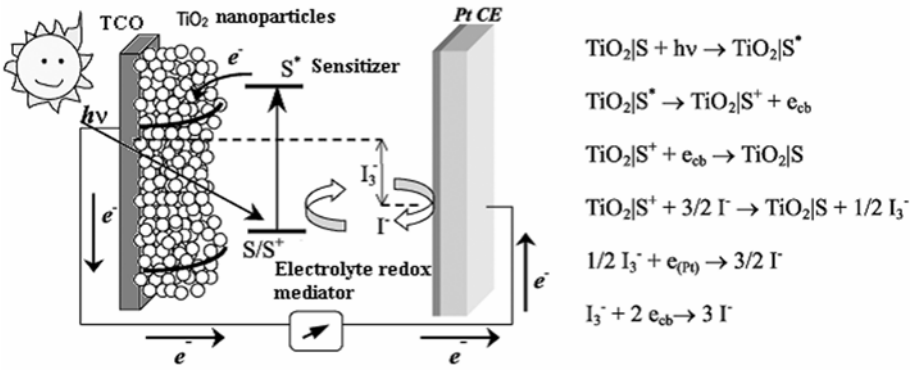

Figure 10. Schematic diagram showing working of DSSC and role of dye.

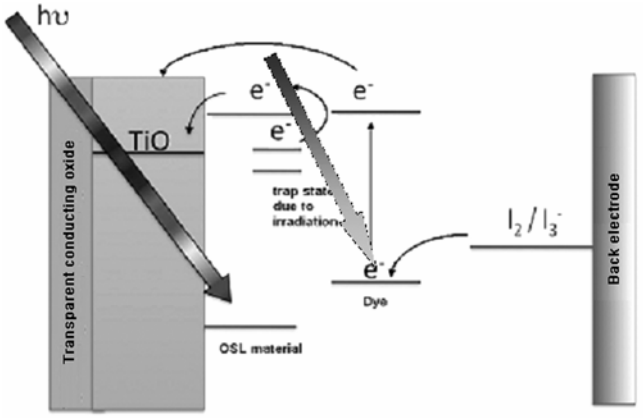

Figure 11. Schematic diagram showing combined action of solid-state absorber and dye in DSSC.

adsorbed on the surface of nanocrystalline TiO_2 particles and an electron from the molecular ground state, S0 is excited to an excited state, S*; (2) the excited electron of the dye is injected into the conduction band of the TiO_2 particles, leaving the dye molecule to an oxidized state, S; (3) the injected electron diffuses through the porous nanocrystalline structure to the transparent conducting oxide (TCO) layer of the glass substrate (negative electrode or anode) and finally through an external load to the counter electrode (positive electrode or cathode); (4) at the counter electrode, the electron is transferred to the triiodide (I_3^-) in electrolyte to yield iodide (I^-) and (5) the cycle is closed through reducing the oxidized dye by the iodide in the electrolyte.

Thus, as explained above, both the dye and the solid-state absorber material contribute to the light harvesting and electron injection events thus, increasing the efficiency of the solar cell. The schematic of the combined action of dye and solid-state absorber is shown in figure 11.

For comparison with a conventional photoelectrode composed of dye modified TiO_2, four types of DSSC were fabricated and cell performance was compared. Tables 2 and 3 summarize the cell parameters for the DSSCs fabricated using two types of photo electrodes; ZnO coated TiO_2 dye modified films (table 2) and films without dye molecule (table 3).

Open circuit voltage (V_{oc} in V), short circuit current (J_{sc} in mA/cm^2), fill factor (%), efficiency (η%) for sample Z1, Z2 and Z3 are tabulated. From this table, we can see that the pristine sample Z1 shows high V_{oc}. This can be because of ZnO acting as the barrier layer since, it is OSL inactive. Among the irradiated samples, Z2 irradiated using 6 MV photon beam showed the maximum efficiency, J_{sc} is increased to 1 mA/cm^2. It is assumed that this irradiation is not creating any new trap centres in the material. Instead, it populates the existing trap centres near the conduction band and upon illumination; the carriers will be injected on to TiO_2, which helps to increase the photocurrent. Also, cracks in the ZnO film can bring dye in direct contact with TiO_2 and contribute to photocurrent. However, there is a slight decrease in the open circuit voltage. But for Z3 sample, which was irradiated with 15 MeV electron beam, the photo current was low. Upon irradiation with the electron beam, radiation-induced trap centres are formed which are deep in the energy gap and the electrons in this trap centre have less probability to be excited to the conduction band and hence, not contributing to the photocurrent.

On comparing with table 2, it is seen that the efficiency is larger for the pristine structures in cell structure without dye molecule (see table 3). From the C–V studies the LUMO of the dye was found to be lying below the conduction band of ZnO, which prevents the injection of electrons from dye to ZnO. In the case of samples without dye, the electrons from both the conduction band and trap centres below it can easily flow to the conduction band of TiO_2 and hence, there is an improvement in the photocurrent for these samples. For 600 cGy (15 MeV) sample, which was irradiated with 15 MeV electron beam, the photo current was low. Upon irradiation with the electron beam radiation induced trap centres are formed which are deep in the energy gap and the electrons in this trap centre have less probability to be excited

Table 4. Photovoltaic measurements of $Al_2O_3:C/TiO_2$ composite with N719 dye.

Sample name	Cell details	V_{oc} (V)	J_{sc} (mA/cm^2)	Fill factor (%)	Efficiency (%)
A1	Pristine	0·487	0·149	32	0·02
A2	600 cGy (6 MV)	0·766	0·528	59	0·24
A3	500 cGy (6 MV)	0·528	0·052	39	0·01

Table 5. Photovoltaic measurements of $Al_2O_3:C/TiO_2$ composite without dye.

Sample name	Cell details	V_{oc} (V)	J_{sc} (mA/cm^2)	Fill factor (%)	Efficiency (%)
A4	Pristine	0·476	0·033	23	0·004
A5	600 cGy (6 MV)	0·488	0·745	28	0·102
A6	500 cGy (6 MV)	0·402	0·181	30	0·022

to the conduction band and hence, not contributing to the photocurrent.

The cell parameters for $Al_2O_3:C/TiO_2$ photoanode are shown in tables 4 and 5. From the table 4, it is clear that the conversion efficiency was larger for the sample A2, which was irradiated with 6 MV photon beam with an absorbed dose of 600 cGy, which can be attributed to the increased OSL property of this sample after irradiation. For sample A3, absorbed dose was insufficient to fill the trap levels.

On comparing with table 4, the efficiency was observed to be lower for the samples without dye (see table 5). As the $Al_2O_3:C$ layer is porous; some of the dye molecules can penetrate through and get into contact with the TiO_2 layer. Upon illumination, electrons from the LUMO of these dye molecules can move to the conduction band of TiO_2. This is in addition to electrons injected from the OSL material. This can be taken as the reason for the improved performance of the cell in presence of the dye. Thus, from the current–voltage analysis of the solar cells, DSSC based on the ZnO/TiO_2 composite electrode gained a J_{sc} of about 1 mA/cm^2 with N719 dye and efficiency of 0·14%, whereas for $Al_2O_3:C/TiO_2$ photoanode structure, the current density was 0·528 mA/cm^2 with N719 dye with an efficiency of 0·24%. The solar cell efficiency values are low and could be due to the TiO_2 layer of the photoanode having inadequate porosity and consequent low dye intake. Recently, our group has attained an efficiency of 7·6% with an optimized photoanode composed of electrospun TiO_2 fibres having embedded graphene (Asha *et al* 2012). Incorporation of these solid-state absorber layers into this optimized photoanode is expected to lead to further improvements.

4. Conclusions

In this work, we present experimental evidence of using OSL materials like ZnO and $Al_2O_3:C$ as an extremely thin solid-state absorber layer in DSSC structure. These nanophosphors were obtained by a simple wet chemical method. Solar cell was fabricated with $ITO/TiO_2/ZnO$ and $ITO/TiO_2/Al_2O_3:C$ as photoanodes with and without incorporating dye molecule. For $ITO/TiO_2/ZnO$ photoelectrode system, it is assumed that the irradiation fills the trap centres in the ZnO, which are injected to the conduction band of TiO_2 upon illumination under AM 1·5 conditions. This process resulted in an increase in photocurrent and hence in the efficiency. For $ITO/TiO_2/Al_2O_3:C$ photoanode, apart from irradiation effects, the $Al_2O_3:C$ is porous and hence, there is a possibility for the dye molecules to diffuse through this layer and reach TiO_2 and this may be the reason for the improved performance. Both ZnO and $Al_2O_3:C$ can be used as solid-state absorbers in conjunction with the dye. On comparing both the dye loaded photoanodes (ZnO/TiO_2 and $Al_2O_3:C/TiO_2$), it can be concluded from the present studies that the $Al_2O_3:C$ is superior to ZnO under photon irradiation. $Al_2O_3:C$ is more sensitive to photon irradiation than ZnO and hence, there can be more trap centres produced in $Al_2O_3:C$. But, further optimizations in the film thickness and irradiation condition (varying the energy and dosage) are needed to enhance the efficiency. Doping the ZnO will also produce additional trap centres, which will improve the OSL phenomenon.

Acknowledgements

The authors acknowledge the Department of Science and Technology, the Government of India for supporting this work. The authors acknowledge the technical help, discussions and assistance for the irradiation experiments from Mr Rajaneesh Kumar and Dr Bhaskaran Pillai, Department of Radiation Oncology, AIMS, Cochin. The authors are also very grateful to Amrita Institute of Medical Sciences (AIMS), for infrastructure support to this programme.

References

Asha A M, Sujith K, Chacko D K, Arun T A, Sivakumar N, Subramanian K R V, Nair A S, Nair S V and Avinash B 2012 *RSC Advances* **2** 13032

Cruz-Vaquez C and Burruel-Ibarra S E 2007 *Radiat. Effects & Defects Solids* **162** 737

Fabregat-Santiago F, Bisquert J and Grätzel M 2009 *J. Am. Chem. Soc.* **131** 558

Ghada I K, Larissa L and Harnik S 2008 *ACS Nano* **2** 833

Gopal K M, Oomman K V and Maggie P 2006 *Solar Energy Mater. & Solar Cells* **90** 75

Grätzel M 2003 *J. Photochem. Photobiol, C Photochem. Rev.* **4** 145

Li S-L, Jiang A K-J and Shaoab K-F 2006 *Chem. Commun.* 2792

Luque A and Martin A 1997 *Phys. Rev. Lett.* **78** 5014

Nozik A J 2002 *Physica* **E14** 115

O'Regan B and Grätzel M 1991 *Nature* **353** 737

Pradhan A S and Lee J I 2008 *J. Med. Phys.* **33** 85

Schaller R D and Klimov V I 2004 *Phys. Rev. Lett.* **92** 186601

Schembri V and Heijmen B J M 2007 *J. Med. Phys.* **34** 2113